Doping dependence of the chemical potential and surface electronic structure in $YBa_2Cu_3O_{6+x}$ and $La_{2-x}Sr_xCuO_4$ using hard x-ray photoemission spectroscopy

Kalobaran Maiti,[1] Jörg Fink,[2,3] Sanne de Jong,[4] Mihaela Gorgoi,[2] Chengtian Lin,[5] Markus Raichle,[5] Vladimir Hinkov,[5] Michael Lambacher,[6] Andreas Erb,[6] and Mark S. Golden[4]

[1]*Department of Condensed Matter Physics and Materials' Science, Tata Institute of Fundamental Research, Homi Bhabha Road, Colaba, Mumbai 400 005, India*

[2]*Helmholtz-Zentrum Berlin, Albert-Einstein-Strasse 15, 12489 Berlin, Germany*

[3]*Leibniz-Institute for Solid State and Materials Research Dresden, P.O. Box 270116, D-01171 Dresden, Germany*

[4]*Van der Waals-Zeeman Institute, University of Amsterdam, NL-1018XE Amsterdam, The Netherlands*

[5]*Max-Planck-Institute for Solid State Research, D-70569 Stuttgart, Germany*

[6]*Walther-Meißner-Institut, Bayerische Akademie der Wissenschaften, Walther-Meißner Strasse 8, 85748 Garching, Germany*

(Received 10 June 2009; published 30 October 2009)

The electronic structure of $YBa_2Cu_3O_{6+x}$ and $La_{2-x}Sr_xCuO_4$ for various values of x has been investigated using hard x-ray photoemission spectroscopy. The experimental results establish that the cleaving of $YBa_2Cu_3O_{6+x}$ compounds occurs predominantly in the $BaCuO_3$ complex, leading to charged surfaces at higher x and to uncharged surfaces at lower x values. The bulk component of the core-level spectra exhibits a shift in binding energy as a function of x, from which a shift of the chemical potential as a function of hole concentration in the CuO_2 layers could be derived. The doping dependence of the chemical potential across the transition from a Mott-Hubbard insulator to a Fermi-liquid-like metal is very different in these two series of compounds. In agreement with previous studies in the literature the chemical-potential shift in $La_{2-x}Sr_xCuO_4$ is close to zero for small hole concentrations. In $YBa_2Cu_3O_{6+x}$, similar to all other doped cuprates studied so far, a strong shift of the chemical potential at low hole doping is detected. However, the results for the inverse charge susceptibility at small x shows a large variation between different doped cuprates. The results are discussed in view of various theoretical models. None of these models turns out to be satisfactory.

DOI: 10.1103/PhysRevB.80.165132 PACS number(s): 71.10.Hf, 71.30.+h, 73.20.−r, 74.25.Jb

I. INTRODUCTION

High-T_c superconductivity in cuprates[1] arises from doping of Mott-Hubbard insulators.[2] The evolution of the electronic structure as a function of doping concentration and the connected metal-insulator transition is still not well understood and may be the central problem of high-T_c superconductivity. Moreover the understanding of the metal-insulator transition of doped Mott-Hubbard insulators as a material class is one of the outstanding challenges occupying contemporary solid-state science. Since in these correlated systems, and in particular in the doped cuprates, there exists a complex interplay between lattice, charge, and spin degrees of freedom, various phases between the antiferromagnetic Mott-Hubbard insulator (or more precisely the charge-transfer insulator) and the paramagnetic Fermi-liquid-like state have been the subject of discussion. The prominent state of matter in this context is the superconducting phase. In the underdoped region the pseudogap phase is also detected, which has been interpreted in terms of preformed pairs,[3] a circulating current phase,[4–7] or exotic fractionalized states with topological order.[8–10] In the underdoped region in many cuprates fluctuating or static "stripe" phases play an important role. These phases are essentially incommensurate unidirectional spin and charge-density waves.[11] In addition, stripelike "nematic" phases have been also predicted[12] and finally observed in cuprates.[13,14]

An interesting question which is related to the changes in the electronic structure of a doped Mott-Hubbard system near the metal-insulator transition is the evolution of the chemical potential μ as a function of electron density n. The rate of the chemical-potential shift $\delta\mu/\delta n$ is equal to the inverse charge susceptibility χ_c^{-1} and is connected to the static compressibility κ of an electron liquid by the relation $\kappa=(1/n^2)(\delta n/\delta\mu)$. Various scenarios have been discussed in relation to the question of the doping dependence of the chemical-potential shift in transition-metal compounds. In a simple doped semiconductor model the chemical potential should jump from the first affinity states to the first ionization states when going from n-type doped to p-type doped systems.[15,16] In the cuprates, the former states correspond to the bottom of the upper Hubbard band while the latter are formed by the Zhang-Rice singlet states[17] (top of the valence band). The energy difference between these states corresponds to the charge-transfer gap which is about 2 eV. Thus a jump of about 2 eV in μ would be expected when going from n- to p-type doped systems or of about 1 eV when going from the undoped system to the heavily p-type doped compound. An alternative scenario is that no shift in μ should occur as a function of doping concentration due to a pinning of the chemical potential at impurity-induced states which are in the gap.[18] A further model for a pinning of the chemical potential is based on a "microscopic" phase separation into a metallic and an insulating phase, e.g., stripe or nematic phases.[11,19]

Various concrete predictions for the chemical-potential shift as a function of the electron density n have been presented in the literature (see, e.g., Ref. 20). For an isotropic Fermi liquid the relation for the rate of the chemical-potential shift

$$\frac{\delta\mu}{\delta n} = \left(\frac{m_b}{m*}\right)\frac{1+F_s^0}{N_b(\mu)} \tag{1}$$

has been given,[21] where m*, m_b, and $N_b(\mu)$ are the effective mass, the bare band mass, and the bare density of states at the chemical potential μ, respectively. F_s^0 is a Landau parameter which represents the isotropic spin-symmetric part of the electron-electron interaction. In an uncorrelated system, $\delta\mu/\delta n$ would be just given by the inverse bare density of state $1/N_b(\mu)$. In correlated systems the effective mass would strongly increase approaching the half-filled case. Thus a very small rate of chemical-potential shift or a very large charge susceptibility $(\delta\mu/\delta n)^{-1}$ would be expected in this approximation. A suppression of the chemical-potential shift has been also predicted by numerical studies in the two-dimensional Hubbard model[21,22] for n_b close to 1, where n_b is the number of electrons in the band. Here, from Monte Carlo studies a relation $\Delta\mu \propto -(n_b-1)^2$ has been arrived at. In addition, a slave boson mean-field analysis of the three-band model yielded a constant chemical potential up to a hole doping $p=1/8$ due to a stripelike phase separation.[23] Finally, based on calculations in the $t-t'-t''-J$ model (which includes the long-range hopping integrals t' and t''), it has been predicted[24] that $\delta\mu/\delta n$ should be small for $t'=0$ and should increase with increasing t'.

Experimentally, the chemical-potential shift can be deduced from core-level shifts in x-ray-induced photoemission spectra (XPS). The reason for this is that the binding energy of the core-level states is measured relative to the chemical potential μ. More explicitly, the shift in the binding energy of the core levels, $\Delta\epsilon$, depends primarily on four terms and can be expressed as

$$\Delta\epsilon = -\Delta\mu + \Delta V_M + K\Delta Q + \Delta E_R, \tag{2}$$

where $\Delta\mu$, ΔV_M, ΔQ, K, and ΔE_R represent the change in chemical potential, the change in the Madelung potential, the change in the valency, a constant, and the change in relaxation energy, respectively.[25] It has turned out that in the cuprates and other transition-metal compounds, for core levels from atoms which do not change their valency upon doping, the terms other than $\Delta\mu$ are small and therefore the chemical-potential shifts can directly be derived from the core-level shifts themselves. This core-level-based method was first applied to the system $Bi_2Sr_2Ca_{1-x}Y_xCu_2O_{8+\delta}$ and a large total shift of the chemical potential of ≈0.8 eV between undoped and overdoped samples was deduced, together with an inverse charge susceptibility $\frac{\delta\mu}{\delta p}|_{p\to 0}$ ≈7 eV/hole for low hole concentration p.[15] For hole concentrations, $p \geq 0.1$ this value was seen to decrease to ≈1 eV/hole.[15] Similar work has been performed on various other cuprates such as $La_{2-x}Sr_xCuO_4$ (Refs. 16 and 26–30), $Nd_{2-x}Ce_xCuO_4$ (Refs. 16 and 31), $Bi_2Sr_2Ca_{1-x}R_xCu_2O_{8+\delta}$ (R=Pr,Er) (Refs. 32 and 33), $Ca_{2-x}Na_xCuO_2Cl_2$ (Ref. 34), and $Bi_2Sr_{2-x}La_xCuO_{6+\delta}$ (Ref. 35). Since the electronic structure close to the Fermi level in all these compounds is determined by doped CuO_2 layers, a universal behavior is expected. However, this is not observed for the p-type doped cuprates since $La_{2-x}Sr_xCuO_4$ shows a negligible $\frac{\delta\mu}{\delta p}|_{p\to 0}$, but all other systems show a large $\frac{\delta\mu}{\delta p}|_{p\to 0} \approx 1.8$ eV/hole.[35] This difference has often been explained in terms of a "microscopic" stripelike phase separation[19] and by the fact that $La_{2-x}Sr_xCuO_4$ or similar compounds in which Sr is replaced by Ba, or La is replaced by Nd or Eu, are much more susceptible to static stripe formation than the other cuprates.[30,31] Alternative explanations of this puzzle have also been discussed in the literature, e.g., the influence of the opening of a pseudogap on the doping dependence of the chemical potential.[29] Finally, based on the above-mentioned calculations in the t-t'-t''-J model it was argued that for $La_{2-x}Sr_xCuO_4$, $\frac{\delta\mu}{\delta p}|_{p\to 0}$ should be small due to its small value of t', while t' for the other cuprate superconductors is larger thus yielding larger $\frac{\delta\mu}{\delta p}|_{p\to 0}$ values.

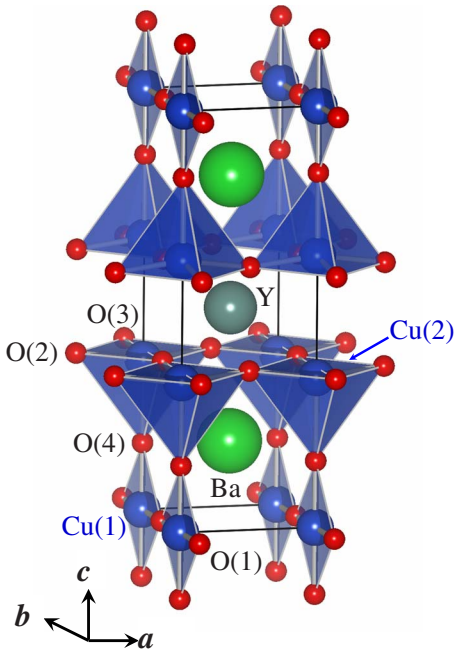

FIG. 1. (Color online) Crystal structure of $YBa_2Cu_3O_7$ (orthorhombic; space group *Pmmm*). O(1) sites are empty in the crystal structure of $YBa_2Cu_3O_6$ leading to a tetragonal structure.

Introducing methods for the determination of chemical-potential shifts, one should also mention that not only core levels but also the Cu $3d^8$ satellite line[16] and the lower Hubbard band[35] have been used as an intrinsic reference system for the determination of the doping dependence of μ.

In this article we apply the core-level binding-energy method to study the chemical-potential shift as a function of doping concentration in a further hole-doped cuprate, namely, $YBa_2Cu_3O_{6+x}$ and compare the results with our own data for the chemical-potential shift of $La_{2-x}Sr_xCuO_4$. $YBa_2Cu_3O_{6+x}$ is an interesting system since it has not only two-dimensional CuO_2 planes which are doped but also one-dimensional CuO_{2+x} units (see below), which transform into metallic ribbons upon increasing the O concentration from 6 to 7. Furthermore, in this context one should mention that $YBa_2Cu_3O_{6+x}$ is the only compound in which nematic stripelike order has been detected in the bulk.[14]

$YBa_2Cu_3O_7$ forms in orthorhombic structure as shown in Fig. 1. As evident in the figure, Y layers are sandwiched by two CuO_2 planes (a,b plane) whereby the latter are believed

to be responsible for superconductivity. The oxygen atoms along the *a* and *b* axes in the CuO_2 planes are denoted by O(2) and O(3), respectively, and are very similar. The copper atoms in the CuO_2 planes are denoted by Cu(2) in the figure. The apical oxygen atoms that—together with the Ba atoms form BaO layers—are denoted by O(4) and the oxygen atoms in the CuO chains along the *b* directions are denoted by O(1). The O(1), O(4), and Cu(1) atoms together form a one-dimensional CuO_3 metallic ribbon.

The decrease in x from $x=1$ to $x=0$ leads to the fragmentation of the chains due to the absence of O(1) atoms and the orthorhombic structure gradually changes near $x=0.3$ to a tetragonal structure.[36,37] Several studies have indicated ordering of oxygen atoms in the chain and/or chain fragments.[38–40]

The other end member, tetragonal $YBa_2Cu_3O_6$, is an antiferromagnetic insulator. In this structure, the Cu(2) atoms are formally divalent, which corresponds to a single hole in the Cu $3d$ shell. In order to yield charge balance, the Cu(1) atoms need to be formally monovalent, i.e., their Cu $3d$ states are completely filled. Evidence of such Cu^{1+} atoms has been observed experimentally in various studies, e.g., by x-ray absorption spectroscopy (XAS).[41]

Increasing x from 0 to 1, i.e., filling the O(1) sites, first the valency of the Cu(1) atoms is changed from monovalent to divalent. This is completed near $x=0.3$. Further increase in x leads to the formation of formally trivalent Cu atoms in the chains and in the planes. Due to the large on-site Coulomb interaction $U \approx 8$ eV for two holes on a single Cu site and the smaller charge-transfer energy $\Delta \approx 3$ eV, the holes are—in reality—not formed at the Cu sites but reside on the adjacent O sites,[42,43] thus forming a Zhang-Rice singlet state together with the already existing hole on the Cu sites.[17] After an insulator to metal transition, the transition into the superconducting phase is subsequently observed. Interestingly, a plateau with superconducting transition temperature T_c of about 60 K for $0.6 \leq x \leq 0.8$ has been observed, which is significantly different from other cuprates. Finally, a maximum T_c of about 91 K is observed for x close to 0.9.[44]

As a reference system for $YBa_2Cu_3O_{6+x}$ we have studied $La_{2-x}Sr_xCuO_4$, which has the K_2NiF_4 structure, where the CuO_2 planes are separated by two LaO layers. La_2CuO_4 is an antiferromagnetic insulator. Divalent Sr substitution at the trivalent La sites leads to hole doping, thereby driving the system metallic. Higher doped compositions near $x=0.15$ exhibit superconductivity at about 40 K.

Photoemission is usually a highly surface sensitive method.[25] For photons having an energy of 1.5 keV (a commonly used x-ray energy in laboratory studies), the mean-free path of the photoelectrons they create is of the order of 20 Å. Increasing the photon energy to higher values reduces the surface sensitivity and leads to results which are more closely related to bulk properties. In addition, the knowledge of which lines are related to the surface and which are related to the bulk is of fundamental importance for XPS studies on the chemical potential as a function of doping concentration. Therefore a prerequisite for our studies of the chemical-potential shift was a detailed investigation of the surface sensitivity of XPS spectra of $YBa_2Cu_3O_{6+x}$ using various photon energies and emission angles.

Cleaving $YBa_2Cu_3O_{6+x}$ crystals perpendicular to the c axis can be performed at three different planes leading to six different possible surface terminations. At present it is not absolutely clear whether the crystals are cleaving predominantly along one plane or whether other cleavage planes or even a mixture of the three possible cleavage planes is occurring, which may lead up to six different terminations on the same cleavage plane. The appearance of specific surface layers may also change as a function of the doping concentration x. Previously, XPS studies on the surface of $YBa_2Cu_3O_{6+x}$ have been published for single crystals,[38,45,46] polycrystalline samples,[47,48] and thin films.[49,50] In this context we also mention scanning tunneling microscopy (STM) (Refs. 51–54) studies on single crystals. More recently, information on the surface of cleaved $YBa_2Cu_3O_{6+x}$ single crystals have been also derived from angle-resolved photoemission spectroscopy (ARPES) studies.[55–64] Most of these investigations of the surface layers of cleaved single crystals indicate that BaO and CuO layers are at the surface, i.e., the cleavage occurs predominately between the BaO layers and the one-dimensional CuO chains. Some authors also discussed a mixed CuO_3/BaO surface termination.[57] On the other hand in theoretical studies on the basis of density-functional calculations (Refs. 65 and 66) it was pointed out that breakage of the strong covalent Cu(1)-O(4) bond would be difficult. STM sudies[52] also reported Y layers at the surface, which would indicate a cleavage between the CuO_2 planes and the Y layers. Finally, cleavage between the BaO and CuO_2 layers have been reported.[55] Recent ARPES studies have also detected overdoped surfaces on cleavage of optimally doped bulk crystals. Such surfaces with doping concentrations different from the bulk are expected when polar surfaces are produced after the cleavage process.

In this article we present first a detailed XPS study of the electronic structure of cleaved $YBa_2Cu_3O_{6+x}$ and $La_{2-x}Sr_xCuO_4$ single crystals. This is followed by the main focus of this contribution: the investigation of the chemical-potential shifts in these systems as a function of their CuO_2 plane doping concentration.

II. EXPERIMENT

High-quality single-phase $YBa_2Cu_3O_{6+x}$ crystals were synthesized by the solution growth method[67] or in nonreactive $BaZrO_3$ crucibles by a self-flux method.[68] The crystals were examined by various other techniques such as inelastic neutron scattering,[14,67] muon spin rotation (μSR),[67] and ARPES.[60,62,63] In Table I we present the doping concentration x, the hole doping p in the CuO_2 layers, the superconducting transition temperatures T_c, and the widths of the superconducting transition temperature ΔT_c. The nontrivial hole doping p for CuO_2 layers was derived from a recent c-axis lattice-parameter study of $YBa_2Cu_3O_{6+x}$ crystals.[69] These values are in qualitative agreement with values derived from XAS measurements on the O $1s$ level on untwinned single crystals.[43] The hole doping concentration for the $x=0.45$ and 0.6 samples have been determined independently to be $p=0.085$ and 0.12, respectively.[13,14] $La_{2-x}Sr_xCuO_4$ crystals were grown with the traveling solvent

TABLE I. Doping concentration x, hole doping p in the CuO_2 layers given per planar Cu atom, T_c (in K) and ΔT_c values (in K) of the $YBa_2Cu_3O_{6+x}$ (YBCO), and $La_{2-x}Sr_xCuO_4$ (LSCO) single crystals used in this work.

	x	p	T_c	ΔT_c
YBCO	0.15	0.006	0	
YBCO	0.45	0.081	35	2–3
YBCO	0.60	0.115	61	1–3
YBCO	0.90	0.165	92	1
YBCO	1.00	0.190	90	1
LSCO	0.00	0	0	
LSCO	0.04	0.04	0	
LSCO	0.10	0.10	26	1.5
LSCO	0.15	0.15	37	1.0
LSCO	0.20	0.20	28	3.0
LSCO	0.30	0.30	0	

zone method.[70] The doping concentration of the crystals together with T_c and ΔT_c is also listed in Table I.

Despite the use of hard x-ray excitation to maximize the bulk sensitivity of our measurements, it is still appropriate to generate a clean surface prior to measurement, and so the single crystals were cleaved in a preparation chamber under a vacuum of $10^{-7}-10^{-9}$ mbar at room temperature by means of removal of a top post immediately before an *in vacuo* transfer to the analysis chamber (base pressure 3×10^{-10} mbar). Only the La_2CuO_4 and $La_{1.7}Sr_{0.3}CuO_4$ samples (i.e., two out of the total of eleven measured doping levels) proved to be uncleavable by this method and were scraped in the preparation chamber using a diamond file prior to the measurements. We observed that the surface cleaning was necessary to obtain clean spectra even if hard x rays were used for spectroscopy.

The XPS measurements were performed at room temperature using the HIKE experimental station at the double crystal monochromator KMC-1 beamline[71] at BESSY, Germany. This beamline operates on a bending magnet and the energy can be scanned in the range of 1.7 to 12 keV. The HIKE end station[72] is equipped with a Gammadata Scienta R-4000 hemispherical electron energy analyzer modified for high transmission and kinetic energies up to 10 keV. The samples were studied using excitation energies of 2010 and 6030 eV with a total-energy resolution of 0.33 and 0.18 eV, respectively. The measurements were taken at grazing incidence of the x-ray beam, while the axis of the spectrometer lens was, within a few degrees, normal to the sample surface. In order to vary surface sensitivity, off-normal-emission spectra were also collected in some cases. Energy referencing was carried out with a combination of measurements of the Fermi cutoff and Au $4f$ levels of a scraped Au foil, held in electrical contact with the samples. The accuracy (and reproducibility) of the absolute and relative energy scales is of the order of 50 meV.

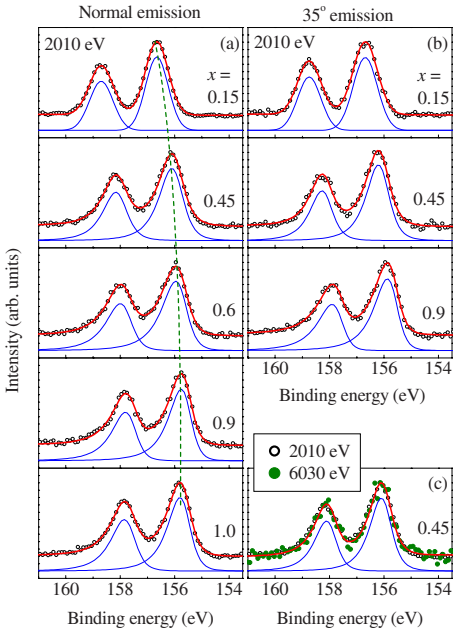

FIG. 2. (Color online) Y $3d$ core-level spectra of $YBa_2Cu_3O_{6+x}$ for various O concentrations. (a) Normal-emission spectra collected with $h\nu$=2010 eV. (b) Analogous spectra collected at the same photon energy but at 35° emission with respect to surface normal. (c) Normal-emission spectra collected with 2010 eV photons (open circles) and 6030 eV photons (closed circles [green in online color version]) for x=0.45. The red solid lines superimposed on the experimental spectra are the total fit results and the thin blue lines represent the spin-orbit split components of the fit.

III. RESULTS

A. $YBa_2Cu_3O_{6+x}$

In Fig. 2, we show the Y $3d$ core-level spectra of $YBa_2Cu_3O_{6+x}$ for the available x values. The spectra collected using 2010 eV photons in normal-emission geometry are shown in the left panel of the figure. All the spectra exhibit a two-peak structure typical of $3d$ core levels with spin-orbit splitting. The lines superimposed on the experimental spectra are the result of a fit comprising two peaks shown by the thin lines below each spectrum. For the asymmetric line shape of these peaks a Pearson IV line shape found in PEAKFIT computer program has been used. The intensity ratio of the two-component peaks is close to 3/2 as expected from the multiplicity of the spin-orbit split features. The component peaks in $YBa_2Cu_3O_{6.15}$ are symmetric and become asymmetric with increasing oxygen concentration. This is the result either of more than one electrostatic screening environment for the Y ions upon hole doping of the CuO_2 planes between which they are sandwiched, or via a mechanism involving coupling of the core hole to a continuum of electron-hole excitations of the charge carriers in the CuO_2 planes.[73]

In addition to this increase in asymmetry, increasing oxygen doping also leads to a clear intensity shift of the spectral energy positions toward lower binding energies. Between x =0.15 and 1 this shift amounts to $\Delta\epsilon$=0.8 eV. The analysis and discussion of this shift will form the focus of Sec. IV B,

dealing with the chemical-potential shifts as a function of doping. Readers, for whom the description of the data from the different core levels—in terms of spectral form and the origin of the feature—would form an activation barrier, are free to jump directly to Sec. IV B and consider Fig. 15, which shows the core-level shift data vs doping.

In order to test whether there is a significant surface component in the Y 3*d* core-level spectra, we have also measured the spectra at an emission angle of 35° with respect to the surface normal and show these data in Fig. 2(b). If we would take the usual "grazing" emission angles of 70° or more, for the high photon energies used here, the signal would become impracticably small (due to the mismatch between the penetration depth of the x rays and the inelastic mean-free-path length of the photoelectrons). Nevertheless, even the moderate emission angle of 35° used here is sufficient to make the experiment more surface sensitive. It is evident from Fig. 2(b) that the spectral line shapes and energy positions of the Y 3*d* features are essentially unchanged compared to those found for normal emission. This would suggest an absence of a surface-related Y 3*d* component. We have tested this hypothesis by measuring the Y 3*d* level for $x=0.45$ with 6030 eV photons in the normal-emission geometry, and plot the hard x-ray data (solid circles) together with those recorded using $h\nu=2010$ eV photons (open circles) in Fig. 2(c). The spectra are identical, establishing that the Y 3*d* core-level profile is devoid of surface-related features, and thus that the $h\nu=2010$ eV data can be considered as wholly bulk representative.

Moving on from the Y 3*d* to the Ba 3*d* and 4*d* spectra, we show the O-doping-dependent data set in Fig. 3. Ba 4*d* spectra collected at normal emission using $h\nu=2010$ eV are shown in Fig. 3(a). Employment of high spectral resolution and good quality crystals reveals distinctly separated features in contrast to earlier data.[45,49,50] The dominant lines at low binding energy clearly shift to lower binding energies with increasing oxygen concentration. The energy shift observed for the Ba core-level lines is significantly larger than that observed in the Y 3*d* spectra shown in Fig. 2. For the Ba case the shift is $\Delta\epsilon=1.2$ eV between $x=0.15$ and 1. Finally, we mention that for the shallow Ba 5*p* core-level excitations (not shown) the same shift has been detected as for the Ba 4*d* levels.

The Ba 4*d* spectra exhibit distinct signatures of multiple features in contrast to their Y 3*d* counterparts. In order to investigate the origin of the clear shoulders visible on the spin-orbit split doublets, we show the Ba 4*d* spectra for $YBa_2Cu_3O_{6.45}$ collected at 35° emission with 2010 eV photon energy, and at normal emission with $h\nu=2010$ and 6030 eV in Fig. 3(b). In this order, the bulk sensitivity of the technique increases. It is clear that in addition to the sharp spin-orbit split features around 87.7 and 90.5 eV binding energies, significant intensity grows gradually around 88.7 and 91.5 eV binding energies upon increasing the surface sensitivity of the measurement. Consequently, these additional high-binding-energy features can be attributed to the core-level spectra from Ba ions situated at the cleavage surface. This trend has also been observed for crystals with other O-doping levels studied in the same manner, spanning right across the higher doping range. The Ba $3d_{5/2}$

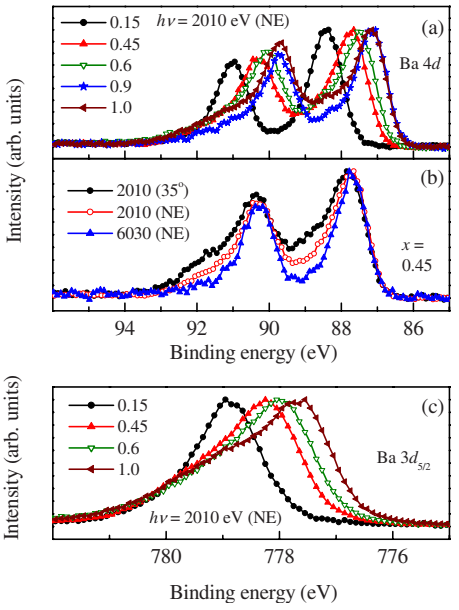

FIG. 3. (Color online) (a) Ba 4*d* core-level spectra $YBa_2Cu_3O_{6+x}$ for various x values collected at normal emission with $h\nu=2010$ eV. (b) Ba 4*d* spectra from $YBa_2Cu_3O_{6.45}$, collected at 35° emission with 2010 eV photons, and at normal emission with both 2010 and 6030 eV excitation energies. (c) A zoom in on the Ba $3d_{5/2}$ spin-orbit split component for various values of x collected at normal emission with $h\nu=2010$ eV.

spectra—of which a portion is shown in Fig. 3(c)—also exhibit similar behavior with respect to the probing depth of the measurement. Figure 3(c) is also well suited to illustrate that the Ba core-level line shape—for a given measurement geometry—also depends on the O concentration, changing from being essentially symmetric for $x=0.15$ to clearly two component for $x=1.0$.

In order to gain a full understanding of the surface-bulk differences seen in the Ba 4*d* spectra, we have fitted the experimental data using asymmetric line shapes after normalization of the Ba 4*d* traces to their total area. The results of the fit are shown in Fig. 4. It is evident that one can simulate the Ba 4*d* spectra of $YBa_2Cu_3O_{6.15}$ collected at 2010 and 6030 eV using one pair of spin-orbit split features. This indicates that the surface-bulk difference felt at the Ba site in this undoped composition is negligible. Further, we note that in every composition, the change in surface sensitivity of the technique leads to significant change in the intensity ratio of the high- to low-binding-energy features; thus clearly establishing that the spin-orbit split feature at higher binding energies is indeed from the sample surface and the lower binding-energy features are from the bulk. In such a case photoemission intensity can be expressed as

$$I(\epsilon) = [1 - e^{-d/\lambda}]I^s(\epsilon) + e^{-d/\lambda}I^b(\epsilon),$$

where d, λ, $I^s(\epsilon)$, and $I^b(\epsilon)$ is the depth of the surface-related layer as shown in Fig. 4, the effective inelastic mean-free-path length, the surface spectrum, and the bulk spectrum, respectively. The first and second terms on the right-hand side of the above equation represent the surface and bulk

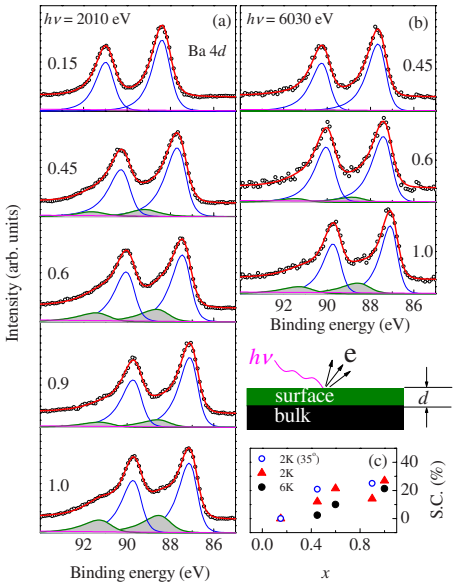

FIG. 4. (Color online) (a) Fits to the Ba 4*d* core-level spectra of $YBa_2Cu_3O_{6+x}$ for various x values collected at normal emission with 2010 eV photon energy. (b) Fits to the Ba 4*d* spectra collected at normal emission with 6030 eV photons. (c) The surface contribution extracted from the fits, as a function of x, whereby the shorthand notation 2K and 6K has been used to designate the use of 2010 and 6030 eV photons, respectively. S.C. represents surface contribution.

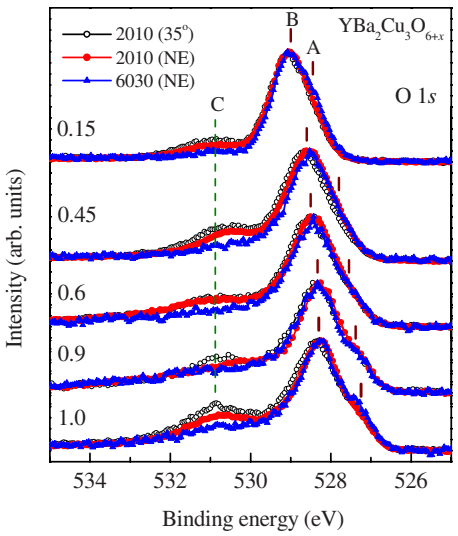

FIG. 5. (Color online) O 1*s* core-level spectra of $YBa_2Cu_3O_{6+x}$ for various x values, collected using the photon energies (and emission angles) indicated, whereby NE stands for normal emission.

contributions to the photoemission spectral function. Various XPS studies indicate that d/λ is about 0.5 for electrons having a kinetic energy of about 1.5 keV ($\lambda \sim 20$ Å), which is also similar to that found in the universal curve.[74–76] Since, $\lambda \propto \sqrt{E_{kin}}$ (E_{kin} is the kinetic energy of the photoelectrons), d/λ for Ba 4*d* photoelectrons is about 0.44 for the spectra corresponding to 2010 eV photons and 0.25 for the spectra corresponding to 6030 eV photons. Thus, the surface contribution in the Ba 4*d* spectra reduces from 36% to 22% with the increase in photon energy. In Fig. 4(c) we observe that the surface contribution (S.C.) gradually increases with increasing x and becomes 25% for $x=1$. This suggests that the cleaved surface contains other contributions in addition to BaO layers, however, the probability of BaO layers at the surface enhances with increasing x.

The O 1*s* core-level spectra recorded for various O concentrations are shown in Fig. 5. All the spectra exhibit three distinct features marked in the figure as A, B, and C. With the reduction in surface sensitivity of the technique (i.e., on going from 35° emission with 2010 eV excitation energy, to normal emission for the same photon energy, to using 6030 eV photons at normal emission), the intensity of the feature C reduces significantly for all the oxygen doping levels studied. This indicates that feature C is associated with surface oxygen atoms.

In order to investigate the origin of multiple features in the O 1*s* spectra in more detail, we have simulated the experimental data using asymmetric line shapes, representing the features A, B, and C. It is evident already from a simple visual inspection of the raw data that a minimum of three features are required to fit the whole spectral region for all the compositions. Thus, to avoid uncertainty in a parameterized fitting procedure, we have adopted a three peak fit guided by a least-squares optimization with respect to the raw data. Two typical cases of fit results are shown in Figs. 6(a) and 6(b), illustrative for all the fits carried out. The doping-dependent change in the areas of the various features is shown in Fig. 6(c) after normalizing the spectra by the total integral area of the bulk features, A and B, to the oxygen content of the compound. First, we observe that the intensity of feature A remains almost unchanged in all the spectra. Feature C is related to the surface oxygen atoms as argued above from its surface sensitivity dependence, and gradually increases with increasing x. The intensity of feature B also gradually increases with increasing x, which indicates a role for the O(1) chain oxygen atoms in the origin of this core-level feature.

The binding energies of the various oxygen atoms in $YBa_2Cu_3O_{7.0}$ have been studied in several calculations[77–79] and using XAS.[43] From these earlier investigations it emerges that O(4) (see Fig. 1) has the lowest binding energy. The binding energies for the couple O(2) and O(3) and lastly O(1) are about 0.7 eV and 0.3 eV, respectively relative to O(4). Therefore, feature A in Figs. 5 and 6 which appears at the lowest binding energy can be attributed to O(4) from the bulk of the crystal. No distinct signatures of the planar oxygen ions O(2) and O(3) and the chain oxygen O(1) could be resolved in the spectra and thus, all three of these O sites contribute to the intensity of peak B. This is perfectly reasonable with regard to the data shown in Fig. 6(c), in which the intensity of feature B grows gradually with x, as can be expected if it is partially O(1) related.

In the final part of this subsection, we present the Cu 2*p* core-level spectra. In the case of $YBa_2Cu_3O_{6+x}$, a simple attribution of each spectral feature to a particular atomic site is severely complicated by a number of factors: first, the existence of two types of Cu site—plane and chain—which take on differing valencies and have differing dimensionali-

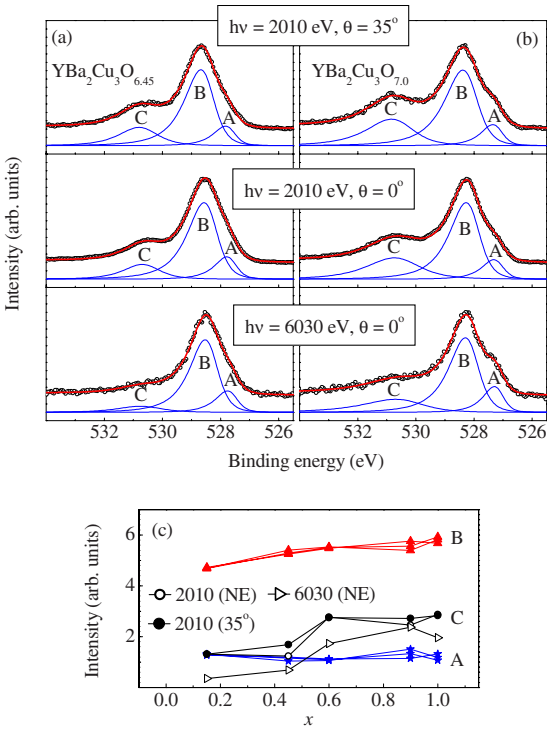

FIG. 6. (Color online) O 1*s* core-level spectra of (a) $YBa_2Cu_3O_{6.45}$ and (b) $YBa_2Cu_3O_{7.0}$ collected under conditions giving differing surface sensitivity. For the panels containing spectra: from top to bottom the bulk sensitivity is increasing. The red (blue) lines represent the simulated total (partial) spectral functions. (c) The areas (i.e., intensities) of the features A, B, and C as a function of x.

ties as a function of O content; second, it is well known that the strong final-state effects visible in the Cu 2*p* spectra of (nearly) divalent cuprate networks are both dependent on the doping level and dimension of the Cu-O structure in question.[80–83]

The Cu 2*p* spectra collected using 2010 eV photons at normal emission are shown in Fig. 7. The data exhibit four spectral features arising from the spin-orbit split $2p_{3/2}$ and $2p_{1/2}$ levels and their satellites. In Fig. 7, the data have been normalized to the area under the $2p_{3/2}$ satellite. Since the spectral line shape of Cu $2p_{1/2}$ is very similar to the line shape of Cu $2p_{3/2}$, we concentrate on the Cu $2p_{3/2}$ features in the following as shown in Fig. 8. In divalent cuprates, the main peak around 933 eV binding energy represents the well-screened final state $|\underline{2p}3d^{10}\underline{L}\rangle$, whereby the intrinsic hole in the 3*d* shell has been pushed away to the ligand atoms (in this case O) due to the positive core-hole potential.[84] The satellite feature, appearing in the binding-energy range of 938–947 eV, corresponds to $|\underline{2p}3d^{9}\rangle$, and is often referred to as the poorly screened final state. The fact that, for the main line, the core-hole screening takes place via charge transfer to the ligands (and also thereby to neighboring CuO_4-plaquettes[15]) means that an analysis of this kind of data offers the opportunity not only to determine parameter values for the model Hamiltonians for the systems in question, but also to study the dynamics of charge transfer in cuprate networks.[80–83,85]

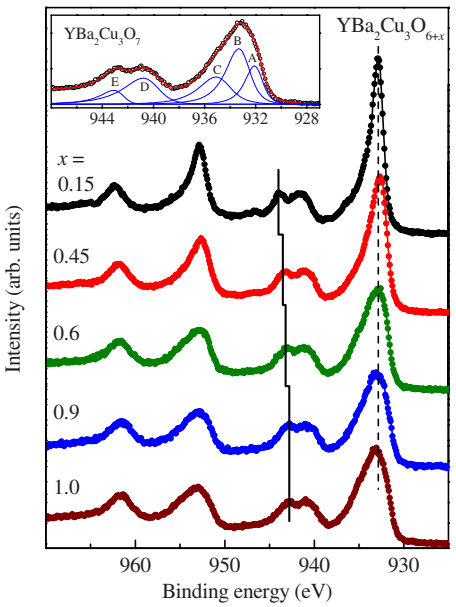

FIG. 7. (Color online) Cu 2*p* spectra of $YBa_2Cu_3O_{6+x}$ for various x values collected at normal emission using 2010 eV photon energy.

Figure 8(a) shows an overlay of a zoomed region of the spectra showing the Cu $2p_{3/2}$ features for the all doping levels studied. Starting with $YBa_2Cu_3O_{6.15}$, as outlined above, Cu(1) is close to monovalent and Cu(2) is divalent. XPS measurements on the monovalent Cu_2O compound[86] show only the well-screened peak and no satellite since the 3*d* shell is already filled in the initial state. Thus the satellite peak for $x=0.15$ is only due to the Cu(2) atoms in the planes,

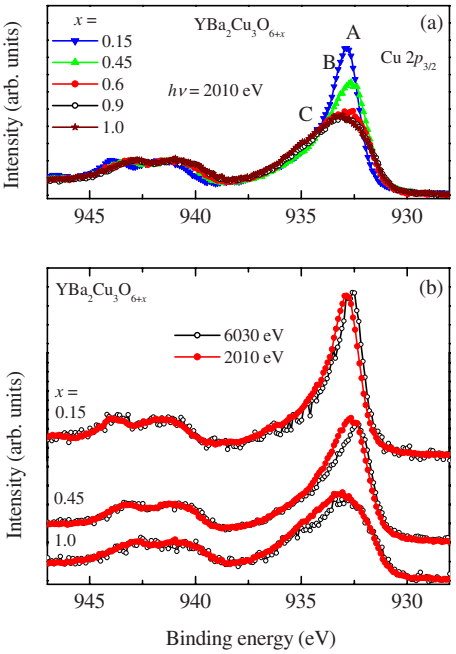

FIG. 8. (Color online) (a) Cu $2p_{3/2}$ spectra from $YBa_2Cu_3O_{6+x}$ for various x values recorded with 2010 eV photons. (b) Analogous data for the doping levels $x=0.15$, 0.45, and 1.0 collected with $h\nu = 2010$ eV and 6030 eV.

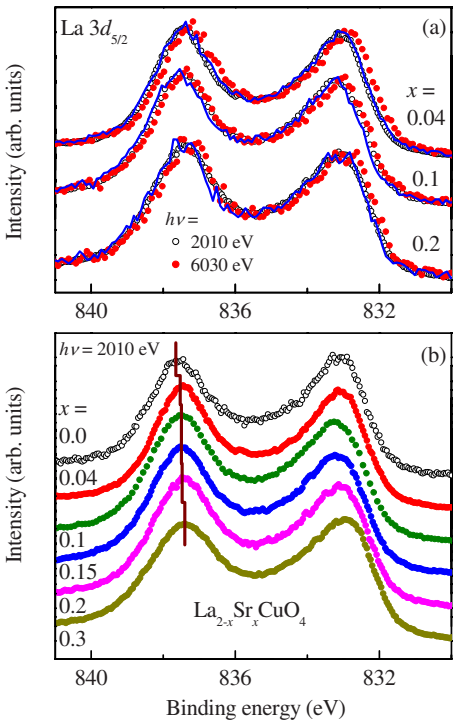

FIG. 9. (Color online) (a) La $3d_{5/2}$ feature and its satellite of $La_{2-x}Sr_xCuO_4$ for various x values are shown for 2010 eV (open circles) and 6030 eV (solid circles) photon energies. The solid line represents the 6030 eV spectra shifted by about 0.2 eV toward higher binding energies. (b) La $3d_{5/2}$ spectra using 2010 eV photons for different values of x.

while the well-screened peak is caused by a sharp Cu(1) peak and a broader Cu(2) peak from the planes. The broadening of the Cu(2) peak is related to various screening channels, more localized ones which come at higher binding energies and more delocalized ones which appear at lower binding energy.[15,83,87]

Further increasing x leads to further oxidation of the Cu(1) atoms, thus increasing the number of divalent Cu at the expense of monovalent Cu. Consequently, the sharp feature within the well-screened peak is reduced and the satellite intensity increases due to divalent Cu in the chains. With increasing x, similar to the Y and Ba core levels discussed above, the binding energy of the satellite moves to lower binding energies. In the context of the chemical-potential shift, this will be discussed in Sec. IV B. The shift of the well-screened peak as a function of x is essentially impossible to evaluate, since various screening channels lead to a complicated structure and the screening conditions also probably change for different x values.

B. $La_{2-x}Sr_xCuO_4$

In Fig. 9, we show the La $3d_{5/2}$ spectra from the different doping levels collected using 2010 and 6030 eV photon energies. Each spectra exhibits two features corresponding to the well-screened main peak at about 833 eV and poorly screened satellite peak at about 837.5 eV binding energies.[88] The line shape of the features does not change with the

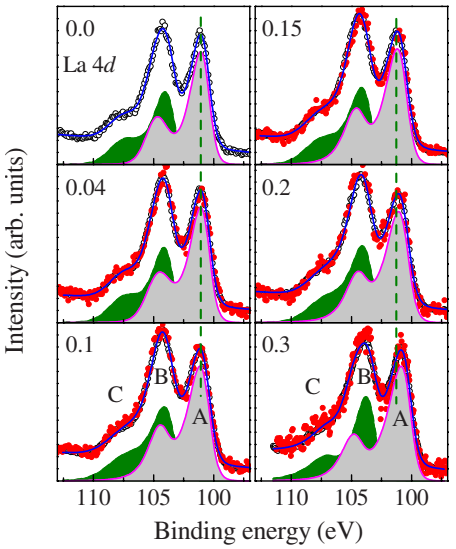

FIG. 10. (Color online) La 4d spectra of $La_{2-x}Sr_xCuO_4$ for various values of x. The open and closed circles represent spectra collected using 2010 and 6030 eV photon energies. The solid line superimposed on the experimental data represent the fit comprising a pair of spin-orbit split doublets, each of which is shown by a green/gray shaded surface.

change in incident photon energy. In order to verify this, we have superimposed the high photon energy spectra [solid line in Fig. 9(a)] by shifting the spectra by about 0.2 eV toward higher binding energies. Evidently the two spectra are very similar. Since the bulk sensitivity of the 6030 eV spectra is significantly higher than the 2010 eV spectra, the above observation suggests that the bulk La 3d features have lower binding energies compared to the surface La 3d spectra. This is very similar to the observations in the Ba core-level spectra in $YBa_2Cu_3O_{6+x}$ samples. This also indicates that the sample surface contains significant amount of La.

In Fig. 9(b), we compare the La $3d_{5/2}$ features corresponding to different doping levels. The vertical lines indicate a guide to the energy shift. The spectra at different doping levels exhibit a small shift in peak positions, indicating finite chemical-potential shifts as observed in earlier studies. In order to verify this, for a La core level with lower intrinsic life time broadening we show the La 4d spectra in Fig. 10. Each spectrum exhibits multiple features. To delineate the origin of various features, we have fit the experimental spectra using a set of doublets, where each doublet represents a main peak and corresponding satellite feature as seen in the La 3d spectra. All the spectra could be simulated remarkably well by two doublets with an intensity ratio of 2:3, which is similar to that expected for the spin-orbit split 4d features. Interestingly, the peak positions estimated in this way reveal an energy shift as a function of doping concentration consistent with the La 3d spectra.

The O 1s spectra collected for various compositions and different bulk sensitivities are shown in Fig. 11. Each spectrum exhibits a two peak structure as demonstrated by fits displayed in Fig. 12. The most intense feature appears at about 528.5 eV binding energy. A change in x leads to a small shift in the peak positions as observed in the La 3d and

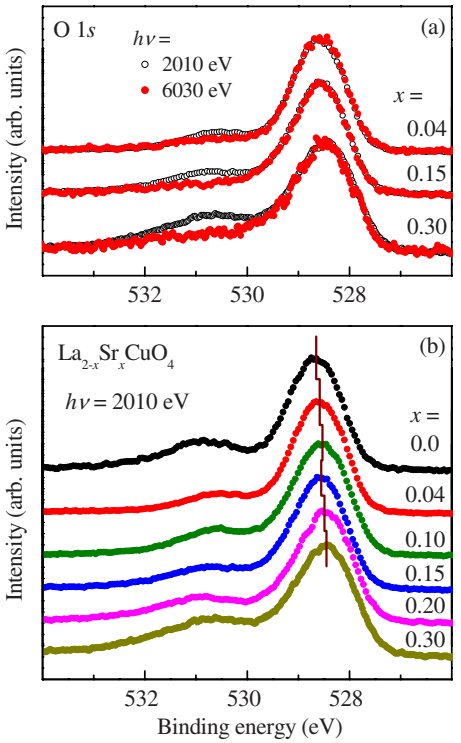

FIG. 11. (Color online) (a) O 1*s* core-level spectra of $La_{2-x}Sr_xCuO_4$ for various *x* values, corresponding to 2010 and 6030 eV photon energies are shown by open and solid circles, respectively. (b) 2010 eV spectra for different values of *x* reveal an energy shift with increasing *x*.

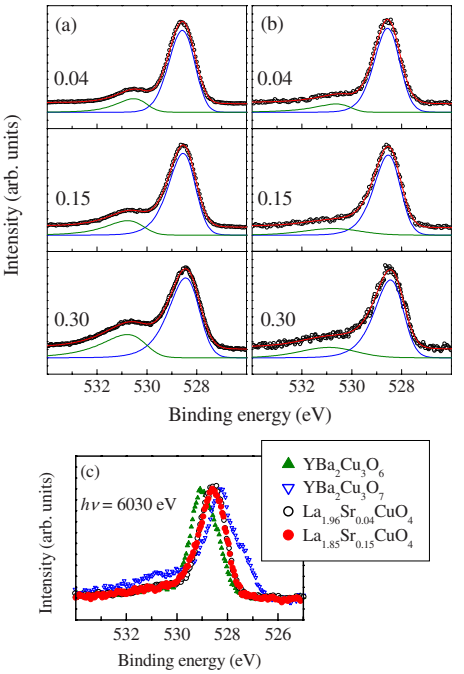

FIG. 12. (Color online) Fit to the O 1*s* features of $La_{2-x}Sr_xCuO_4$ for various *x* values obtained at (a) 2010 eV and (b) 6030 eV photon energies exhibiting two distinct features in all the cases. (c) The peak position and profiles of the O 1*s* spectra in $La_{2-x}Sr_xCuO_4$ are compared to those of the two $YBa_2Cu_3O_7$ end members.

4*d* signals. The feature at about 531 eV binding energy, often attributed to an impurity feature, reduces significantly with increasing bulk sensitivity of the technique. However, this feature does not vanish even if the surface is well prepared by vacuum cleaving of high quality single crystals and hard x-ray excitation is used. Thus, this again questions its relation to impurities, raising the possibility that it is an intrinsic feature due to surface oxygen atoms as also observed in $YBa_2Cu_3O_{6+x}$ samples [see Fig. 12(c)].

In Fig. 13, we show the Cu $2p_{3/2}$ signals corresponding to 2010 eV incident photon energies for different values of *x*. As described above for the case of $YBa_2Cu_3O_{6+x}$ the satellite feature corresponds to the nonscreened excitation. Interestingly, similar to the La 3*d* and 4*d* and O 1*s* core-level spectra a small shift in binding energy of the satellite feature is detected with the change in *x* (see Fig. 13).

In Fig. 14 we compare the spectra obtained with 2010 and 6030 eV photon energies. The spectra are normalized to the intensity of the satellite features. In this case there is no energy shift visible in the satellite feature. In addition, the satellite features remain unaffected even though the technique becomes significantly bulk sensitive at $h\nu$=6030 eV, establishing again the local character of this feature.

In contrast the main peak exhibits significant redistribution of spectral weight with increasing bulk sensitivity. Three features can be identified in the spectra and are marked with A, B, and C in Fig. 14. Feature C represents locally screened final states (whereby the ligand hole resides in the CuO_4 plaquette containing the core hole) and remains almost unchanged in both the spectra. Features A and B, which are caused by more delocalized screening channels, are changing when changing the surface sensitivity in the measurements, attesting to different Cu environments in the surface and bulk regions of the sample.

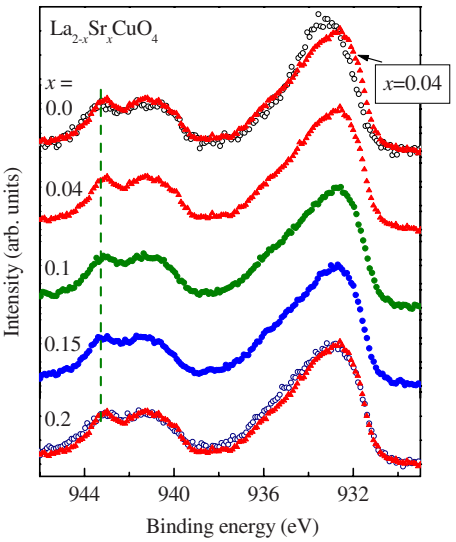

FIG. 13. (Color online) Cu $2p_{3/2}$ spectra of $La_{2-x}Sr_xCuO_4$ for various values of *x* measured with a photon energy of 2010 eV. While the satellite position shows only a small shift, the main peak exhibits significant change. The data for x=0.0 and 0.2 are superimposed with data for x=0.04 (red triangles).

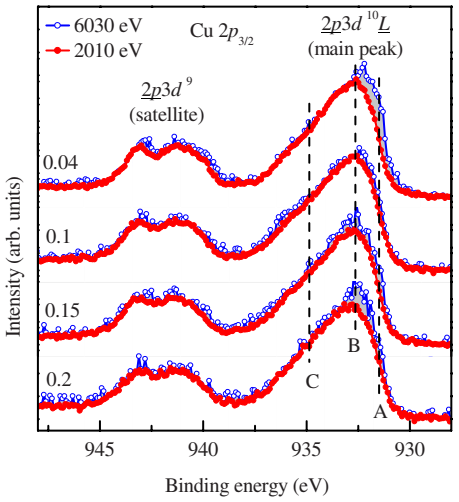

FIG. 14. (Color online) Cu $2p_{3/2}$ spectra of $La_{2-x}Sr_xCuO_4$ for various x values collected using 2010 eV (solid circles) and 6030 eV (open circles) photons. A distinct signature of three features A, B, and C is visible in the spectra of the main line region.

IV. DISCUSSION

A. Surface electronic structure

At the beginning of this discussion on the electronic structure of cleaved cuprate crystals (which starts by dealing with the case of $YBa_2Cu_3O_{6+x}$), we emphasize that in the present XPS experiments we have no spatial resolution. The diameter of the photon beam is of the order of 500 μm. Thus we obtain only averaged information from the surface which may, on a microscopic scale, possess differing terminations. On the other hand, due to the possibility of using photon energies between 2010 and 6030 eV and by using different emission angles, depth sensitive information has been obtained, which can be used to differentiate between the surface and bulk electronic structure. In previous work on cleaved $YBa_2Cu_3O_{6+x}$ single crystals (see e.g., Ref. 46) it was pointed out that core-level excitations (except Cu $2p$) have a low binding-energy component, which represents bulk properties, and high binding components, which are caused by surface contaminations and by intrinsic surface contributions. Unfortunately the two high binding-energy components appear almost at the same energy.

As pointed out in Sec. III A, we see core-level excitations from atoms where spectra show no sensitivity to the changes in the probing depth of the experiment, and others which show a dependence. Examples for the latter are the Ba and O core-level excitations, while the former type is illustrated by the core lines from Y and the poorly screened final-state satellite feature for Cu.

The lack of a high binding-energy peak in the Y $3d$ spectra enables us to conclude that the portion of the surface terminations containing Y layers is negligible. Furthermore, we have never observed any spin-orbit doublet for Y shifted by 1.5 eV to higher binding energies as has been detected in air-exposed samples.[46] This indicates that we do not have any Y-related surface contamination. The slight asymmetry of the lines at higher doping levels can be fully understood by a Doniach-Sunjic-like screening of the core holes by the metallic CuO_2 layers, which are in close proximity to the Y site.

For the Ba $3d$ and $4d$ core-level excitations we observe only one spin-orbit doublet at low O concentrations, with symmetric lines which we ascribe to Ba atoms in the bulk. At higher O concentrations we see shoulders at higher binding energies. The question is whether this second component is related to an intrinsic surface component or to surface contamination. In a previous study, air-exposed samples show a strong high-energy component shifted by 1.5 eV compared to the bulk component.[46] This could indicate that the high-energy component in the spectra may be caused by carbonate or hydroxide formation due to reaction with species in the residual vacuum. On the other hand, we see no increase in the high binding-energy component as a function of time. Therefore it is unlikely that this component is related to contamination due to reactions with a background pressure in the 10^{-10} mbar range, or during the brief interval between cleavage at ca. 10^{-8} mbar and transfer to the analysis chamber. We thus assign the high binding-energy component to an intrinsic surface layer and thus conclude that Ba must be there in the terminating layer. From our measurements we cannot obtain detailed information on the possibly reconstructed BaO-CuO-BaO complex at the crystal termination after cleavage. At present it is also less clear why the surface layer in the crystals with low O concentration does not produce the high binding-energy component, although a connection to the population of the O(1) sites in the chains is a clear possibility. From the present measurements it follows that the cleavage plane or the reconstruction that may follow cleavage probably changes between low x values and high x values. The spectra also indicate that for low x values there are no charged surface layers (which would produce a high binding-energy component in the XPS spectra), while for higher doping levels, a charged surface layer exists. The latter results are in line with the detection of overdoped surface layers in ARPES spectra of $YBa_2Cu_3O_{6+x}$ for higher x values.[61,62,64]

The O $1s$ spectra are also composed of a high binding-energy component and a low binding-energy component with a clear fine structure in the form of a shoulder at low binding energy. In Sec. III A, the signal below 530 eV was ascribed to bulk O ions, with O(4) giving rise to the low binding-energy shoulder and the other three sites adding up to give the strongest feature at ca. 529 eV. At high photon energy ($h\nu$=6030 eV) and in particular for small x values the intensity of the high-binding-energy component (binding energy >530 eV) is rather small. This indicates that using similar arguments as those discussed in the case of the Ba core levels, this part of the O $1s$ spectrum is related to an intrinsic surface contribution.

In the Cu $2p$ spectra, upon changing the surface sensitivity, no changes in the satellite features could be detected. This is in line with the interpretation of this feature in terms of atomiclike excitations. Small differences in the main lines are observed, which could reflect small differences in the screening channels between the bulk and the surface. On the other hand, we point out that the changes in the main line of $YBa_2Cu_3O_{6+x}$ upon changing the photon energy are less pro-

nounced than in $La_{2-x}Sr_xCuO_4$ and, as will be discussed in a moment, is even less pronounced than in $Nd_{2+x}Ce_xCuO_4$.

In the following we discuss the spectra of $La_{2-x}Sr_xCuO_4$. The common view is that cleavage occurs between the LaO layers, thus forming LaO terminated surfaces. Interestingly, in the La core-level spectra taken with different surface sensitivities, no surface component could be detected. Only a small shift of about 200 meV could be detected between spectra taken with $h\nu$=2010 eV and 6030 eV. This shift may be caused by a Madelung potential at the La sites that may be different for the surface layer and the bulk.

In principle, the bulk component in the O 1*s* spectra at low binding energy should be a superposition of two lines stemming from the CuO_2 plane O atoms and the apical O sites. Although we are performing high-resolution XPS experiments, the two sites could not be resolved, indicating that the binding energy of the O 1*s* levels of the two sites is almost the same. The high-energy component in the O 1*s* spectra in $La_{2-x}Sr_xCuO_4$ shows a strong surface sensitivity, almost disappearing in the spectra taken with the photon energy $h\nu$=6030 eV. This means that similar to the case of $YBa_2Cu_3O_{6+x}$, the high-energy component is surface related. In the data from the cleaved crystals (x=0.04 to 0.2) this component is small, while for the scraped crystals (x=0 and 0.3) the high-energy component is considerably larger. The enhanced roughness of the scraped surface leads to larger surface contributions than for the cleaved surface. Thus, the larger high-binding-energy feature in the O 1*s* spectra from the scraped sample surfaces re-establishes its connection to the surface electronic structure.

As mentioned previously the satellite feature in the Cu 2*p* spectra does not change when changing the surface sensitivity of the XPS measurements using different photon energies, in keeping with its atomiclike multiplet character. On the other hand, in the main line the low energy features A and B in Fig. 14 increase when measured with increased bulk sensitivity. These features are caused from more delocalized screening channels, in which the hole on the (oxygen) ligands moves further away, forming Zhang-Rice singlets. In a first approximation these screening channels would come from the in-plane electronic structure of the CuO_2 layers and therefore it is difficult to understand why there should be a difference between a surface CuO_2 layer and a bulk CuO_2 layer. On the other hand such an enhancement with increasing bulk sensitivity was also observed in earlier studies, in particular for $Nd_{2+x}Ce_xCuO_4$ (Ref. 89). This could indicate that an explanation of the well-screened feature solely in terms of in-plane screening channels is probably not sufficient. Possibly the total three-dimensional electronic structure has to be used in the framework of an Anderson impurity model to calculate the screening channels for the Cu 2*p* core hole to obtain a satisfactory description of the spectra.[83,87,90]

B. Chemical-potential shift vs doping level

Now that we have successfully identified lines from core-level excitations in the XPS spectra which are definitely related to the bulk properties and which are not influenced by surface effects, we can evaluate the bulk core-level binding energies as a function of doping. Since the core-level binding energies are measured relative to the Fermi level, we can extract the chemical potential as a function of hole concentration as was described in Sec. I. In the following, we discuss our results on the chemical-potential shifts and compare them with theoretical calculations and previous experimental results published in the literature.

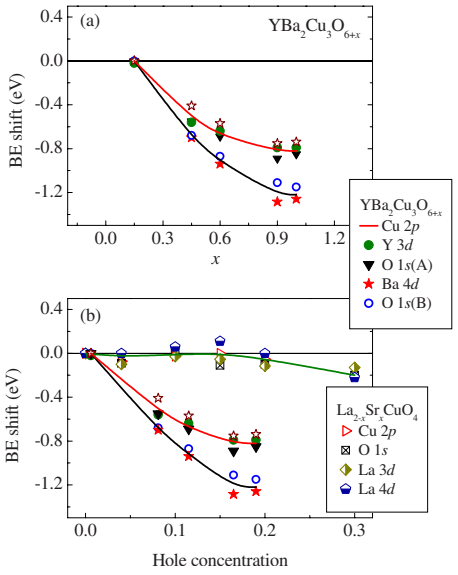

FIG. 15. (Color online) binding-energy shift of the various bulk-related core-levels lines as a function of (a) x and of (b) hole concentration in the CuO_2 layers in $YBa_2Cu_3O_{6+x}$ samples. The analogous energy shifts for $La_{2-x}Sr_xCuO_4$ samples are also shown in (b). The solid lines represent a guide to the eye.

Without further ado, in Fig. 15 we show a compilation of all of the relevant data for our single-crystal-only bulk sensitive study of $YBa_2Cu_3O_{6+x}$ and $La_{2-x}Sr_xCuO_4$. The top panel shows the shift in the binding energy of the core levels indicated relative to that of x=0.15 vs x in $YBa_2Cu_3O_{6+x}$. The bottom panel shows the binding-energy shifts vs the hole concentration p per Cu ion in the CuO_2 planes. In Fig. 15(b) we also compare these data with core-level shifts derived in $La_{2-x}Sr_xCuO_4$ for various $x=p$ values. For both systems the binding-energy shift values are given relative to p =0.

In $La_{2-x}Sr_xCuO_4$ the core-level excitations from O, La, and Cu atoms show *no* shift up to and including p=0.15. For higher p values a negative shift is detected (i.e., the binding energy of the core levels, referred to the Fermi energy is decreasing) which reaches a value of 0.2 eV for p=0.3. Our results are in perfect agreement with the data published in Ref. 28. The fact that the shifts $\Delta\epsilon$ are zero for $p \leq 0.15$ may be interpreted by an accidental cancellation of the four terms in Eq. (2) in this Sr concentration range. However, we believe that such a cancellation for three different atoms in such a large concentration range is rather unlikely. Thus we assume that in Eq. (2) the Madelung term, the on-site valency term, and the relaxation term are negligible for the particular core-level features under consideration, and that the observed shift is determined by the chemical-potential

shift $\Delta\mu$. We note here that, contrary to previous investigations, we have determined the energy shift for the Cu $2p$ lines not from the main line but from the satellite and thus avoid "contamination" of the core-level shift values with chemical shift terms related to the changing copper valence. For the O atoms the situation is less clear since the holes which are formed upon doping with Sr are situated mainly on the O sites, as a result of the formation of Zhang-Rice singlets. Thus, the $2p$ count on the O sites will be changed, and a chemical shift of the O $1s$ core level should be expected. Apparently, the constant K in Eq. (2) is too small to enable the detection of this shift. The calculated Madelung terms in a point-charge model are of the order of 2 eV for doping concentrations up to $x=0.2$ (see Ref. 30). Opposite shifts are derived from these calculations for Cu vs La and O core-level excitations. On the other hand, these calculated values are probably strongly reduced by a high background dielectric constant. This assumption is supported by the experimental fact for the core levels of the three types of atoms, the same shift (or no shift) is observed, independent of the distance to the dopant atoms (here Sr). Turning to the last term in Eq. (2), it is plausible that the relaxation energies do not significantly depend on the doping concentration because the observed core-level shifts for atoms in metallic CuO_2 layers and insulating LaO layers are shown to be the same. We also emphasize that the three different types of atoms are bonded quite differently. For La and O in the LaO planes a predominantly ionic bonding is a reasonable starting point, whereas Cu and O in the CuO_2 planes are expected to show a strong covalent bonding component. Thus the results for $La_{2-x}Sr_xCuO_4$ would indicate that the chemical potential is pinned by impurity levels within the charge-transfer gap when going from the undoped insulating system to the doped metallic system. More precisely, the inverse charge susceptibility $\delta\mu/\delta p$ is zero for $0 \leq p \leq 0.15$.

For $YBa_2Cu_3O_{6+x}$ the results for the chemical-potential shift are completely different to those of $La_{2-x}Sr_xCuO_4$ [see Fig. 15(b)]. Interpreting the measured core-level shifts in terms of a chemical-potential shift, we obtain from the data for $p<0.1$, presented in Fig. 15(b), an inverse charge susceptibility $\frac{\delta\mu}{\delta p}|_{p\to 0}$ between 5.5 and 9.5 eV/hole depending which core-level lines one considers. This would support the simple semiconductor scenario in which upon doping the Fermi level moves from the center of the gap rapidly into the valence band (effective lower Hubbard band in a single band model). At higher hole concentration ($p \geq 0.15$) the shift seems to saturate. For one group of core-level excitations the maximum shift saturates at -0.8 eV while for others a maximum shift of -1.2 eV is detected. The lower value would correspond reasonably to half of the gap between the valence band and the upper Hubbard band in the insulating system. The higher saturation value is slightly too big when compared to half of the gap. This could indicate that the values from the Ba $4d$ and the O $1s$(B) excitations are in some way less directly related to the (bulk) chemical-potential shift. It is remarkable that these two excitations both stem from the BaO(4) plane, while the other excitations predominantly stem from the CuO_2-Y-CuO_2 complex [except the small contribution from the O(1) atoms in the CuO(1) chains]. Having said that, it is still unclear as to why the behavior of the core-level shifts should group in this manner. *A priori* we would have expected that the shifts from the ionic atoms such as Ba and Y and from the Cu $2p$ satellite would be the same. The large shifts of the Ba core-level excitations as a function of doping were also discussed in Ref. 46, however, without a possible chemical-potential shift being taken into account. Both the Ba and the O(4) atoms are close to the O(1) dopant atoms and possibly experience an additional negative shift due to a Madelung term caused by the increasing number of O(1) atoms. Since the Cu(1) atoms contribute only 1/3 to the Cu $2p$ spectra this effect is possibly not detected in the Cu $2p_{3/2}$ spectra. In this context one should also mention that in these Cu $2p_{3/2}$ spectra, the Cu(1) atoms only contribute to the satellite for p larger than ≈ 0.3 since for lower p values they are monovalent and therefore do not form a satellite feature.

In view of the discussions above, we tentatively assign the chemical-potential shift in this compound to values measured via the Cu $2p$, Y $3d$, and O $1s$ (line A) core-level excitations. We then come to a value for the inverse charge susceptibility $\frac{\delta\mu}{\delta p}|_{p\to 0} \approx 5.5$ eV/hole.

This nonzero value is in agreement with values derived in previous studies. In Ref. 15 an inverse charge susceptibility $\frac{\delta\mu}{\delta p}|_{p\to 0} \approx 7$ eV/hole has been derived for the system $Bi_2Sr_2Ca_{1-x}Y_xCu_2O_{8+\delta}$, which saturates for $p>0.1$. The total shift between $p=0$ and $p=0.25$ amounts to $\Delta\mu=0.8$ eV. On the other hand in Ref. 35 a "universal" inverse charge susceptibility $\frac{\delta\mu}{\delta p}|_{p\to 0} \approx 1.8$ eV/hole has been observed for various non-$La_{2-x}Sr_xCuO_4$ cuprates [$Bi_2Sr_2Ca_{1-x}R_xCu_2O_{8+\delta}$($R$ =Pr,Er), $Ca_{2-x}Na_xCuO_2Cl_2$, and $Bi_2Sr_{2-x}La_xCuO_{6+\delta}$]. Thus we are left with two puzzles: (i) why is $La_{2-x}Sr_xCuO_4$ the only p-type doped cuprate which shows a negligible inverse charge susceptibility for small p and (ii) why are the inverse charge susceptibilities of the non-$La_{2-x}Sr_xCuO_4$ systems so different?

To begin with we deal with the second puzzle. For the various cuprates, the energy bands near the Fermi level originating from the CuO_2 planes are fairly similar.[79] In this way we could understand why our values $\frac{\delta\mu}{\delta p}|_{p\to 0}$ and $\Delta\mu$ between $p=0$ and $p=0.2$ for $YBa_2Cu_3O_{6+x}$ agree reasonably with the values for $Bi_2Sr_2Ca_{1-x}Y_xCu_2O_{8+\delta}$ presented in Ref. 15. On the other hand, it is difficult to understand why $YBa_2Cu_3O_{6+x}$ has such a different inverse charge susceptibility when compared with the "universal" curve derived in Ref. 35. One way to explain this discrepancy would be taking into account the formation of CuO_3 chains, only existing in $YBa_2Cu_3O_{6+x}$. On the other hand, for small x values we start with the $CuO(4)_2$ dumbbells, which upon doping, i.e., insertion of O(1) atoms, form more and more fragmented chains which cause localized states, also close to the Fermi level.[79] Upon completely filling the chains, a Cu(1)$3d_{y^2-z^2}$-O(1)$2p_y$-O(4)$2p_z$ band is formed, which is similar to the CuO_2 layer bands. In addition, close to the Fermi level another chain band occurs which is caused by a π hybridization of O $2p$ orbitals of the O(1) and O(4) atoms. Both this band and the localized states formed by the fragmented chains would be more likely to cause pinning of the chemical potential, leading to a smaller chemical-potential shift but not an increase in the

inverse charge susceptibility. Therefore it is difficult to understand why the inverse charge susceptibility detected in $YBa_2Cu_3O_{6+x}$ in the present experiments is so much larger than in the other cuprates studied in Ref. 35. In this context we also mention that this large chemical-potential shift in $YBa_2Cu_3O_{6+x}$ is not due to formation of metallic CuO_3 chains before the insulator-metal transition appears in the CuO_2 planes. XAS measurements on untwinned single crystals clearly indicate that the number of holes in both CuO units shows almost the same doping dependence.[43] This indicates, when considering the dimensionality of the two units, that the insulator-metal transition comes first in the planes and later in the chains, meaning that the observed chemical-potential shift for low doping in the CuO_2 planes is not determined by the chains but by the planes. Finally, in this context we mention measurements of the plasmon dispersion by electron energy-loss spectroscopy.[91–93] The dispersion coefficient extracted from those measurements yield information on the momentum-dependent compressibility of the electron liquid. For the two compounds $YBa_2Cu_3O_7$ and $Bi_2Sr_2CaCu_2O_8$ almost the same dispersion coefficient has been detected, which fits the $YBa_2Cu_3O_{6+x}/Bi_2Sr_2Ca_{1-x}Y_xCu_2O_{8+\delta}$ agreement for the chemical-potential shift we observe, but raises questions why Er and Pr-doped $Bi_2Sr_2CaCu_2O_{8+\delta}$ and La-doped $Bi_2Sr_2CuO_{6+\delta}$ appears to be different in their carefully conducted XPS experiments.

We have confirmed in this work earlier results for a zero inverse charge susceptibility for $La_{2-x}Sr_xCuO_4$ for small x values (see Ref. 28). In addition, in our present work we have discovered a further system which shows a large inverse charge susceptibility, but which is even larger than in various other non-$La_{2-x}Sr_xCuO_4$ compounds. As pointed out in Sec. I various models for the existence or nonexistence of a finite inverse charge susceptibility have been proposed.

Several theoretical calculations[20,94,95] have predicted for a p-type doped Mott-Hubbard insulator the appearance of a quasiparticle like resonance at the top of the lower Hubbard band. This would give a jump of the chemical-potential shift $\Delta\mu = U/2$. In a charge-transfer insulator (which can be transformed into an effective Mott-Hubbard insulator) the shift would be half of the charge-transfer gap. These calculations also predict that the resonances move into the gap depending on the size of U relative to a critical value U_c. Such a shift could reduce the inverse charge susceptibility as experimentally observed in the system $La_{2-x}Sr_xCuO_4$. On the other hand, in view of the similarities of the crystal structure and the electronic structure of the CuO_2 planes in the various cuprate high-T_c superconductors, it is very difficult to understand why the parameters determining the energy position of the quasiparticle resonance should be so different for the various compounds.

Another reason for a vanishing chemical-potential shift upon doping a Mott-Hubbard insulator could be a phase separation into a metallic and an insulating phase. Microscopic phase separation has been claimed to be detected in the stripe phases in which antiferromagnetic insulating antiphase domains are separated by periodically spaced domain walls to which the holes segregate (see e.g., Ref. 19). Actually, as mentioned in Sec. I, a slave boson mean-field analysis of the three-band model resulted in a constant chemical potential up to $p=1/8$. At this doping concentration—corresponding to four lattice constants in the CuO_2 plane—the cuprates are most susceptible to stripe formation. Below this doping concentration, the distance between the rivers of charge increase more and more, leaving the hole concentration within the microscopic metallic regions (the stripes) unchanged. This could lead to a vanishing chemical-potential shift, an argument which was used for the explanation of the zero inverse charge susceptibility observed in $La_{2-x}Sr_xCuO_4$ (Ref. 30). Above $p=1/8$ the common view is that in the stripe phase, the doping concentration within the stripes increases. In this scenario based on microscopic phase separation not only the vanishing chemical-potential shift for $La_{2-x}Sr_xCuO_4$ for small x was explained but also the reduced $\delta\mu/\delta p$ for $R_{1-x}A_xMnO_3$ (R: rare earth; A: alkaline earth) around the charge ordered composition range.[96] In addition, the fixed chemical potential in $La_{2-x}Sr_xNiO_4$ for $x \leq 0.4$ (Refs. 30 and 97] was also discussed in this context.

On the other hand, we see serious problems to explain the vanishing chemical-potential shift in $La_{2-x}Sr_xCuO_4$ for small x on the basis of a microscopic phase separation, as, in this compound only fluctuating stripes have been observed. Only in the systems $La_{2-x}Sr_xCuO_4$ in which part of La is replaced by Nd or Eu, or Sr is replaced by Ba, have static stripes been detected. Furthermore, for $x=0.15$ we are definitely in a range with strongly interacting stripes, which is a region far from that discussed in terms of microscopic phase separation. Finally, in this scenario it is very difficult to explain the difference between $La_{2-x}Sr_xCuO_4$ and $YBa_2Cu_3O_{6+x}$ as regards the core-level shifts since in the former system only fluctuating stripes exist, while in the latter system a nematic stripe liquid has even been detected experimentally for $x=0.45$ (Ref. 14).

Another explanation of the anomalous inverse charge susceptibility in $La_{2-x}Sr_xCuO_4$ is based on the role of the next-nearest-neighbor hopping integral t' in the band dispersion of cuprates. Theoretical work going in this direction was published in Ref. 24 predicting an increasing chemical-potential shift with increasing t'. This scenario is related to the van Hove singularity close to the Fermi surface of the two-dimensional electronic structure of the CuO_2 planes. This singularity causes a high density of states close to the Fermi level, which in turn may reduce the chemical-potential shift. For a small t'/t (t is the nearest-neighbor hopping integral) causing a square Fermi surface, the chemical potential lies in the singularity and doping causes only a small shift. Larger absolute t'/t values shift the singularity below the Fermi level, thus increasing the chemical-potential shifts caused by small doping concentrations. On the other hand, a compilation of t'/t values based on band-structure calculations[98] shows that t'/t for La_2CuO_4 is considerably larger than that of $Ca_2CuO_2Cl_2$. This would give a smaller chemical-potential shift for the latter when compared with the former in clear contradiction with the experimental findings. Moreover, the band-structure calculations and also ARPES data indicate that in all the cuprates t'/t is finite, shifting the van Hove singularity well below the Fermi level. Thus a doping concentration near 0.2 is needed to shift the chemical potential into the singularity which could reduce

the chemical-potential shift. In a recent paper,[35] therefore, a doping-dependent t'/t has been introduced to explain the small $\frac{\delta\mu}{\delta p}|_{p\to 0}$ in $La_{2-x}Sr_xCuO_4$.

For completeness we also mention discussions of the influence of a pseudogap on the chemical-potential shift in doped cuprates.[30,32] Since the observed pseudogaps in the underdoped cuprates are of the order of 60 meV they have a negligible influence on the chemical-potential shifts detected in this work. Furthermore the existence of a pseudogap in underdoped cuprates is a generic phenomenon and cannot therefore explain the differences in the chemical-potential shifts between different cuprates, which were discussed above.

V. CONCLUSIONS

We have studied the core-level spectra of $La_{2-x}Sr_xCuO_4$ and $YBa_2Cu_3O_{6+x}$ samples for different values of x using high-resolution hard x-ray photoemission spectroscopy with variable photon energies up to 6030 eV. In those spectra we could separate core-level features derived only from the bulk and features which come from the surface. The latter seem predominantly caused by intrinsic surface contributions, i.e., contributions which are related to the cleaving of the surface which leads to reconstructions and charge redistributions at the surface, and only a small part seems due to surface contamination. The experimental results establish that the cleavage in $YBa_2Cu_3O_{6+x}$ crystals for $x \geq 0.45$ occurs predominantly in the $BaO(1)Cu(1)O(4)_2$ layers, which result in charged terminations. For small x values the cleavage planes are found to be again in the $Cu(1)O(4)_2$ layers, thus leading in this case to a negligible contribution from charged surface terminations.

Evaluating the binding energies of the core levels from the unambiguously bulk-related features we could determine the chemical-potential shifts as a function of the doping concentration in the CuO_2 planes. For $La_{2-x}Sr_xCuO_4$ we could confirm previous results in the literature indicating no shift of the chemical potential up to and including a doping concentration $x=0.15$. In view of a simple picture of a doped Mott-Hubbard insulator, a large jump of the chemical potential of the order of half the gap energies, i.e., of the order of 0.8 eV is expected. In $YBa_2Cu_3O_{6+x}$, on the other hand this expected large shift is detected when going from the underdoped material to the optimally doped high-T_c superconductor. The observed concentration dependence of the chemical-potential shift is in good agreement with that observed in $Bi_2Sr_2Ca_{1-x}Y_xCu_2O_{8+\delta}$.[15] However, this shift is considerably larger than that in three other doped cuprate systems presented in the literature.[35] In particular the changes in the chemical-potential shift per hole, i.e., the inverse charge susceptibility for small x values, differ considerably between different (non-$La_{2-x}Sr_xCuO_4$) p-type doped cuprates. These contradicting results are discussed in terms of different scenarios which could influence the chemical-potential shift as a function of doping: the influence of microscopic charge separation (stripe formation), particular band-structure phenomena such as the influence of the next-nearest-neighbor hopping integral t', or the pseudogap. None of these scenarios yield a satisfactory explanation covering the detected experimental results. Therefore, although we embarked on this systematic, bulk sensitive study of the doping dependence of the chemical potential μ in $YBa_2Cu_3O_{6+x}$ and $La_{2-x}Sr_xCuO_4$ in order to achieve a generically valid picture for this fundamental property of these electron systems, we are obliged to close this paper with the call for further experimental and theoretical work that still seems to be necessary to understand the ongoing chemical-potential puzzle in the cuprates.

ACKNOWLEDGMENTS

J.F. is grateful for discussions with M. Vojta. We acknowledge technical assistance by F. Schäfers. K.M. acknowledges the Alexander von Humboldt Stiftung, Germany and the Leibniz-Institute for Solid State and Materials Research, Dresden, Germany for financial assistance. J.F., V.H., and A.E. appreciate financial support by the DFG (Forschergruppe Grant No. FOR 538). This work is part of the research program of the "Stichting voor Fundamenteel Onderzoek der Materie (FOM)," which is financially supported by the "Nederlandse Organisatie voor Wetenschappelijk Onderzoek (NWO)." This work was supported by the European Community-Research Infrastructure Action under the FP6 "Structuring the European Research Area" Programme (through the Integrated Infrastructure Initiative "Integrating Activity on Synchroton and Free Electron Laser Science"–Contract No. R II 3-CT-2004-506008).

[1] J. G. Bednorz and K. A. Müller, Z. Phys. B **64**, 189 (1986).
[2] M. Imada, A. Fujimori, and Y. Tokura, Rev. Mod. Phys. **70**, 1039 (1998).
[3] H. B. Yang, J. D. Rameau, P. D. Johnson, T. Valla, A. Tsvelik, and G. D. Gu, Nature (London) **456**, 77 (2008).
[4] S. Chakravarty, R. B. Laughlin, D. K. Morr, and C. Nayak, Phys. Rev. B **63**, 094503 (2001).
[5] C. M. Varma, Phys. Rev. Lett. **83**, 3538 (1999).
[6] M. E. Simon and C. M. Varma, Phys. Rev. Lett. **89**, 247003 (2002).
[7] B. Fauque, Y. Sidis, V. Hinkov, S. Pailhes, C. T. Lin, X. Chaud, and P. Bourges, Phys. Rev. Lett. **96**, 197001 (2006).
[8] S. Sachdev, Rev. Mod. Phys. **75**, 913 (2003).
[9] P. A. Lee, N. Nagaosa, and X. G. Wen, Rev. Mod. Phys. **78**, 17 (2006).
[10] P. A. Lee, Rep. Prog. Phys. **71**, 012501 (2008).
[11] V. J. Emery, S. A. Kivelson, and J. M. Tranquada, Proc. Natl. Acad. Sci. U.S.A. **96**, 8814 (1999).
[12] S. A. Kivelson, E. Fradkin, and V. J. Emery, Nature (London) **393**, 550 (1998).
[13] V. Hinkov, P. Bourges, S. Pailhes, Y. Sidis, A. Ivanov, C. D. Frost, T. G. Perring, C. T. Lin, D. P. Chen, and B. Keimer, Nat.

Phys. **3**, 780 (2007).
[14] V. Hinkov, D. Haug, B. Fauque, P. Bourges, Y. Sidis, A. Ivanov, C. Bernhard, C. T. Lin, and B. Keimer, Science **319**, 597 (2008).
[15] M. A. van Veenendaal, R. Schlatmann, G. A. Sawatzky, and W. A. Groen, Phys. Rev. B **47**, 446 (1993).
[16] P. G. Steeneken, L. H. Tjeng, G. A. Sawatzky, A. Tanaka, O. Tjernberg, G. Ghiringhelli, N. B. Brookes, A. A. Nugroho, and A. A. Menovsky, Phys. Rev. Lett. **90**, 247005 (2003).
[17] F. C. Zhang and T. M. Rice, Phys. Rev. B **37**, 3759 (1988).
[18] J. W. Allen *et al.*, Phys. Rev. Lett. **64**, 595 (1990).
[19] M. Vojta, Adv. Phys. **58**, 564 (2009).
[20] A. Georges, G. Kotliar, W. Krauth, and M. J. Rozenberg, Rev. Mod. Phys. **68**, 13 (1996).
[21] N. Furukawa and M. Imada, J. Phys. Soc. Jpn. **62**, 2557 (1993).
[22] E. Dagotto, A. Moreo, F. Ortolani, J. Riera, and D. J. Scalapino, Phys. Rev. Lett. **67**, 1918 (1991).
[23] J. Lorenzana and G. Seibold, Phys. Rev. Lett. **89**, 136401 (2002).
[24] T. Tohyama and S. Maekawa, Phys. Rev. B **67**, 092509 (2003).
[25] S. Hüfner, *Photoelectron Spectroscopy* (Springer Verlag, Berlin, 1995).
[26] G. Rietveld, M. Glastra, and D. Vandermarel, Physica C **241**, 257 (1995).
[27] A. Fujimori, K. Morikawa, A. Ino, and T. Mizokawa, J. Electron Spectrosc. Relat. Phenom. **78**, 31 (1996).
[28] A. Ino, T. Mizokawa, A. Fujimori, K. Tamasaku, H. Eisaki, S. Uchida, T. Kimura, T. Sasagawa, and K. Kishio, Phys. Rev. Lett. **79**, 2101 (1997).
[29] A. Fujimori *et al.*, J. Phys. Chem. Solids **59**, 1892 (1998).
[30] A. Fujimori, A. Ino, J. Matsuno, T. Yoshida, K. Tanaka, and T. Mizokawa, J. Electron Spectrosc. Relat. Phenom. **124**, 127 (2002).
[31] N. Harima, J. Matsuno, A. Fujimori, Y. Onose, Y. Taguchi, and Y. Tokura, Phys. Rev. B **64**, 220507(R) (2001).
[32] O. Tjernberg, H. Nylen, G. Chiaia, S. Soderholm, U. O. Karlsson, M. Qvarford, I. Lindau, C. Puglia, N. Martensson, and L. Leonyuk, Phys. Rev. Lett. **79**, 499 (1997).
[33] N. Harima, A. Fujimori, T. Sugaya, and I. Terasaki, Phys. Rev. B **67**, 172501 (2003).
[34] H. Yagi, T. Yoshida, A. Fujimori, Y. Kohsaka, M. Misawa, T. Sasagawa, H. Takagi, M. Azuma, and M. Takano, Phys. Rev. B **73**, 172503 (2006).
[35] M. Hashimoto *et al.*, Phys. Rev. B **77**, 094516 (2008).
[36] P. K. Gallagher, H. Obryan, S. Sunshine, and D. Murphy, Mater. Res. Bull. **22**, 995 (1987).
[37] H. Verweij, Solid State Commun. **67**, 109 (1988).
[38] J. D. Jorgensen, B. W. Veal, A. P. Paulikas, L. J. Nowicki, G. W. Crabtree, H. Claus, and W. K. Kwok, Phys. Rev. B **41**, 1863 (1990).
[39] D. J. Werder, C. H. Chen, R. J. Cava, and B. Batlogg, Phys. Rev. B **38**, 5130 (1988).
[40] R. Sonntag, D. Hohlwein, T. Bruckel, and G. Collin, Phys. Rev. Lett. **66**, 1497 (1991).
[41] J. M. Tranquada, S. M. Heald, A. R. Moodenbaugh, and Y. W. Xu, Phys. Rev. B **38**, 8893 (1988).
[42] N. Nücker, J. Fink, J. C. Fuggle, P. J. Durham, and W. M. Temmerman, Phys. Rev. B **37**, 5158 (1988).
[43] N. Nücker, E. Pellegrin, P. Schweiss, J. Fink, S. L. Molodtsov, C. T. Simmons, G. Kaindl, W. Frentrup, A. Erb, and G. Muller-Vogt, Phys. Rev. B **51**, 8529 (1995).
[44] R. J. Cava, B. Batlogg, C. H. Chen, E. A. Rietman, S. Zahurak, and D. Werder, Nature (London) **329**, 423 (1987).
[45] D. E. Fowler, C. R. Brundle, J. Lerczak, and F. Holtzberg, J. Electron Spectrosc. Relat. Phenom. **52**, 323 (1990).
[46] C. R. Brundle and D. E. Fowler, Surf. Sci. Rep. **19**, 143 (1993).
[47] P. Steiner, V. Kinsinger, I. Sander, B. Siegwart, S. Hufner, and C. Politis, Z. Phys. B **67**, 19 (1987).
[48] P. Srivastava, B. R. Sekhar, N. Saini, S. K. Sharma, K. B. Garg, B. Mercey, P. Lecoeur, and H. Murray, Solid State Commun. **88**, 105 (1993).
[49] G. Frank, C. Ziegler, and W. Gopel, Phys. Rev. B **43**, 2828 (1991).
[50] Y. A. Teterin, Physica C **212**, 306 (1993).
[51] H. L. Edwards, J. T. Markert, and A. L. de Lozanne, Phys. Rev. Lett. **69**, 2967 (1992).
[52] H. You, U. Welp, G. W. Crabtree, Y. Fang, S. K. Sinha, J. D. Axe, X. Jiang, and S. C. Moss, Phys. Rev. B **45**, 5107 (1992).
[53] D. J. Derro, E. W. Hudson, K. M. Lang, S. H. Pan, J. C. Davis, J. T. Markert, and A. L. de Lozanne, Phys. Rev. Lett. **88**, 097002 (2002).
[54] M. Maki, T. Nishizaki, K. Shibata, and N. Kobayashi, Phys. Rev. B **65**, 140511(R) (2002).
[55] N. Schroeder, R. Bottner, S. Ratz, E. Dietz, U. Gerhardt, and T. Wolf, Phys. Rev. B **47**, 5287 (1993).
[56] N. Schroeder, R. Bottner, S. Ratz, S. Marquardt, E. Dietz, U. Gerhardt, and T. Wolf, Solid State Commun. **87**, 277 (1993).
[57] M. C. Schabel, C. H. Park, A. Matsuura, Z. X. Shen, D. A. Bonn, R. Liang, and W. N. Hardy, Phys. Rev. B **57**, 6090 (1998).
[58] M. C. Schabel, C. H. Park, A. Matsuura, Z. X. Shen, D. A. Bonn, R. Liang, and W. N. Hardy, Phys. Rev. B **57**, 6107 (1998).
[59] T. Kondo *et al.*, Phys. Rev. Lett. **98**, 157002 (2007).
[60] S. V. Borisenko *et al.*, Phys. Rev. Lett. **96**, 117004 (2006).
[61] K. Nakayama, T. Sato, K. Terashima, H. Matsui, T. Takahashi, M. Kubota, K. Ono, T. Nishizaki, Y. Takahashi, and N. Kobayashi, Phys. Rev. B **75**, 014513 (2007).
[62] V. B. Zabolotnyy *et al.*, Phys. Rev. B **76**, 064519 (2007).
[63] V. B. Zabolotnyy *et al.*, Phys. Rev. B **76**, 024502 (2007).
[64] M. A. Hossain *et al.*, Nat. Phys. **4**, 527 (2008).
[65] C. Calandra, F. Manghi, and T. Minerva, Phys. Rev. B **46**, 3600 (1992).
[66] C. Calandra and F. Manghi, J. Electron Spectrosc. Relat. Phenom. **66**, 453 (1994).
[67] V. Hinkov, S. Pailhes, P. Bourges, Y. Sidis, A. Ivanov, A. Kulakov, C. T. Lin, D. P. Chen, C. Bernhard, and B. Keimer, Nature (London) **430**, 650 (2004).
[68] A. Erb, E. Walker, and R. Flukiger, Physica C **258**, 9 (1996).
[69] R. Liang, D. A. Bonn, and W. N. Hardy, Phys. Rev. B **73**, 180505(R) (2006).
[70] M. Lambacher, Ph.D. thesis, TU Munich, 2008.
[71] F. Schaefers, M. Mertin, and M. Gorgoi, Rev. Sci. Instrum. **78**, 123102 (2007).
[72] M. Gorgoi *et al.*, Nucl. Instrum. Methods Phys. Res. A **601**, 48 (2009).
[73] S. Doniach and M. Sunjic, J. Phys. C **3**, 285 (1970).
[74] K. Maiti and R. S. Singh, Phys. Rev. B **71**, 161102(R) (2005).
[75] K. Maiti, U. Manju, S. Ray, P. Mahadevan, I. H. Inoue, C. Carbone, and D. D. Sarma, Phys. Rev. B **73**, 052508 (2006).
[76] R. S. Singh, V. R. R. Medicherla, K. Maiti, and E. V. Sampathkumaran, Phys. Rev. B **77**, 201102(R) (2008).

[77] H. Krakauer, W. E. Pickett, and R. E. Cohen, J. Supercond. **1**, 111 (1988).
[78] J. Zaanen, M. Alouani, and O. Jepsen, Phys. Rev. B **40**, 837 (1989).
[79] W. E. Pickett, Rev. Mod. Phys. **61**, 433 (1989).
[80] T. Böske *et al.*, Phys. Rev. B **57**, 138 (1998).
[81] K. Maiti, D. Sarma, T. Mizokawa, and A. Fujimori, Europhys. Lett. **37**, 359 (1997).
[82] K. Maiti, D. D. Sarma, T. Mizokawa, and A. Fujimori, Phys. Rev. B **57**, 1572 (1998).
[83] A. Koitzsch *et al.*, Phys. Rev. B **66**, 024519 (2002).
[84] S. Larsson, Chem. Phys. Lett. **32**, 401 (1975).
[85] M. S. Golden, C. Dürr, A. Koitzsch, S. Legner, Z. W. Hu, S. Borisenko, M. Knupfer, and J. Fink, J. Electron Spectrosc. Relat. Phenom. **117-118**, 203 (2001).
[86] N. Nücker, J. Fink, B. Renker, D. Ewert, C. Politis, P. J. W. Weijs, and J. C. Fuggle, Z. Phys. B **67**, 9 (1987).
[87] K. Karlsson, O. Gunnarsson, and O. Jepsen, Phys. Rev. Lett. **82**, 3528 (1999).
[88] J. C. Fuggle, F. U. Hillebrecht, Z. Zolnierek, R. Lasser, C. Freiburg, O. Gunnarsson, and K. Schonhammer, Phys. Rev. B **27**, 7330 (1983).
[89] M. Taguchi *et al.*, Phys. Rev. Lett. **95**, 177002 (2005).
[90] K. Karlsson, O. Gunnarsson, and O. Jepsen, Int. J. Mod. Phys. B **14**, 3791 (2000).
[91] N. Nücker, H. Romberg, X. X. Xi, J. Fink, B. Gegenheimer, and Z. X. Zhao, Phys. Rev. B **39**, 6619 (1989).
[92] S. Nakai, N. Nücker, H. Romberg, M. Alexander, and J. Fink, Phys. Scr. **41**, 596 (1990).
[93] H. Romberg, N. Nücker, J. Fink, T. Wolf, X. X. Xi, B. Koch, H. P. Geserich, M. Durrler, W. Assmus, and B. Gegenheimer, Z. Phys. B **78**, 367 (1990).
[94] D. S. Fisher, G. Kotliar, and G. Moeller, Phys. Rev. B **52**, 17112 (1995).
[95] H. Kajueter and G. Kotliar, Phys. Rev. Lett. **77**, 131 (1996).
[96] K. Ebata, M. Takizawa, A. Fujimori, H. Kuwahara, Y. Tomioka, and Y. Tokura, Phys. Rev. B **78**, 020406(R) (2008).
[97] M. Satake, K. Kobayashi, T. Mizokawa, A. Fujimori, T. Tanabe, T. Katsufuji, and Y. Tokura, Phys. Rev. B **61**, 15515 (2000).
[98] E. Pavarini, I. Dasgupta, T. Saha-Dasgupta, O. Jepsen, and O. K. Andersen, Phys. Rev. Lett. **87**, 047003 (2001).